THE ASTROPHYSICAL JOURNAL, 646:L127–L130, 2006 August 1

HIGH-J $v = 0$ SiS MASER EMISSION IN IRC +10216: A NEW CASE OF INFRARED OVERLAPS

J. P. FONFRÍA EXPÓSITO, M. AGÚNDEZ, B. TERCERO, J. R. PARDO, AND J. CERNICHARO
Departamento de Astrofísica Molecular e Infrarroja, Instituto de Estructura de la Materia, CSIC,
Calle Serrano 121, E-28006 Madrid, Spain
Received 2006 May 29; accepted 2006 June 22; published 2006 July 25

ABSTRACT

We report on the first detection of maser emission in the $J = 11$–10, $J = 14$–13, and $J = 15$–14 transitions of the $v = 0$ vibrational state of SiS toward the carbon-rich star IRC +10216. These masers seem to be produced in the very inhomogeneous region between the star and the inner dust formation zone, located at $\simeq(5$–$7)R_*$, with expansion velocities below 10 km s^{-1}. We interpret the pumping mechanism as being due to overlaps between $v = 1$–0 rovibrational lines of SiS and mid-IR lines of C_2H_2, HCN, and their ^{13}C isotopologues. The large number of overlaps found suggest the existence of strong masers for high-J $v = 0$ and $v = 1$ SiS transitions, located in the submillimeter range. In addition, it could be possible to find several rotational lines of the SiS isotopologues displaying maser emission.

Subject headings: circumstellar matter — masers — stars: AGB and post-AGB — stars: carbon

Online material: color figure

1. INTRODUCTION

The detection of strong maser emission at the frequencies of pure rotational transitions of some molecules is a common phenomenon in circumstellar envelopes (CSEs) of evolved stars (Elitzur 1992; Gray 1999). The maser is usually produced in a small region of the envelope and sometimes provides valuable information on the physical conditions of the emitting region.

Because of the different chemistry, masers are produced by different molecules in O- and C-rich stars. In O-rich stars, SiO exhibits strong maser emission in different rotational transitions within several vibrational states, from $v = 1$ to $v = 4$ (Cernicharo et al. 1993; Pardo et al. 1998). These masers are formed in a region of the CSE very close to the stellar surface and seem to be driven by near-IR radiation (Pardo et al. 2004). In C-rich stars, although SiO is present with similar abundances to those in O-rich stars (Schöier et al. 2006), no SiO maser has been detected. The explanation could be that SiO is formed at $\simeq(3$–$5)R_*$ (Agúndez & Cernicharo 2006), where the angular dilution of the star is high and the density and temperature are lower than in the regions where SiO masers are produced in O-rich stars. In C-rich stars, only HCN shows strong maser emission, in several pure rotational lines within vibrational states from $\nu_2 = 1$ to $\nu_2 = 4$ (Lucas & Cernicharo 1989; Schilke & Menten 2003). These masers must be formed in the innermost regions of the CSE. SiS has been previously found to show weak maser emission in the $v = 0$, $J = 1$–0 transition in IRC +10216 (Henkel et al. 1983).

In this Letter, we report on the first detection of maser emission from the $J = 11$–10, $J = 14$–13, and $J = 15$–14 transitions in the $v = 0$ vibrational state of SiS (hereafter M_1, M_2, and M_3) observed toward the C-rich star IRC +10216. We have also obtained observations of $v = 1$ rotational lines that exhibit thermal emission. We propose that overlaps of $v = 1$–0 rovibrational transitions of SiS with mid-IR lines of C_2H_2 and HCN could provide the pumping mechanism for these masers, as well as higher J, $v = 0$ SiS masers in the submillimeter range. This discovery is interesting because this species could play a role in C-rich stars similar to that of SiO in O-rich stars: the energy level pattern of both molecules is similar, and it is also formed close to the star, as chemical equilibrium and interferometric observations imply (Bieging & Nguyen-Q-Rieu 1989).

2. OBSERVATIONS

The observations of the $v = 0$, $J = 6$–5 and $J = 8$–7 to $J = 15$–14 transitions of SiS (see Fig. 1, *left*) were carried out on 2004 June 19 with the IRAM 30 m radio telescope, at phase $\phi_{IR} \simeq -0.05$ (Monnier et al. 1998). Four SIS receivers operating at 3, 2, 1.3, and 1 mm were used simultaneously. System temperatures were 120–225 K for the 3 and 2 mm receivers and 200–600 K for the 1.3 and 1 mm receivers. Atmospheric opacities ranged between 0.08 at 108 GHz and 0.2 at 272 GHz. For the $J = 10$–9 SiS line at 181.5 GHz, the system temperature was significantly higher, $\simeq 10^4$ K, because of proximity to the atmospheric water line at 183.3 GHz. The intensity scale was calibrated using two absorbers at different temperatures according to the atmospheric transmission model ATM (Cernicharo 1985; Pardo et al. 2001). Pointing and focus were regularly checked on the nearby quasar OJ 287. The observations were made in wobbling mode, with 180″ offset and the secondary nutating at a rate of 0.5 Hz. The back ends were a filter bank with 256 MHz bandwidth and 1 MHz resolution and an autocorrelator with 80 kHz resolution ($\Delta v \simeq 0.08$–0.2 km s^{-1}). The lines of SiS in the $v = 1$ state (see Fig. 1, *right*) were also observed with the IRAM 30 m telescope between 1989 and 2001.

In addition, we show some spectra corresponding to rovibrational lines of SiS (see Fig. 1, *center*) from a mid-IR high-resolution spectrum (11–14 μm) obtained in 2002 December with the TEXES spectrometer mounted on the 3 m Infrared Telescope Facility (observational procedures described in Lacy et al. 2002; J. P. Fonfría Expósito et al. 2006, in preparation).

3. RESULTS AND DISCUSSION

The $v = 1$ rotational lines show single-cusped profiles, and their relative intensities indicate that the rotational levels are thermally populated. The line widths correspond to expansion velocities of 9–11 km s^{-1}, lower than the terminal velocity of $\simeq$14.5 km s^{-1} (Cernicharo et al. 2000), and thus the emission arises from the innermost region of the CSE, between the photosphere and the inner dust formation zone, located at $\simeq 5R_*$ (J. P. Fonfría Expósito et al. 2006, in preparation; Keady & Ridgway 1993). We can derive the SiS abundance in that region from the $v = 1$ lines assuming a uniform sphere at a distance of 180 pc with a radius of $10R_*$, illuminated by the central star

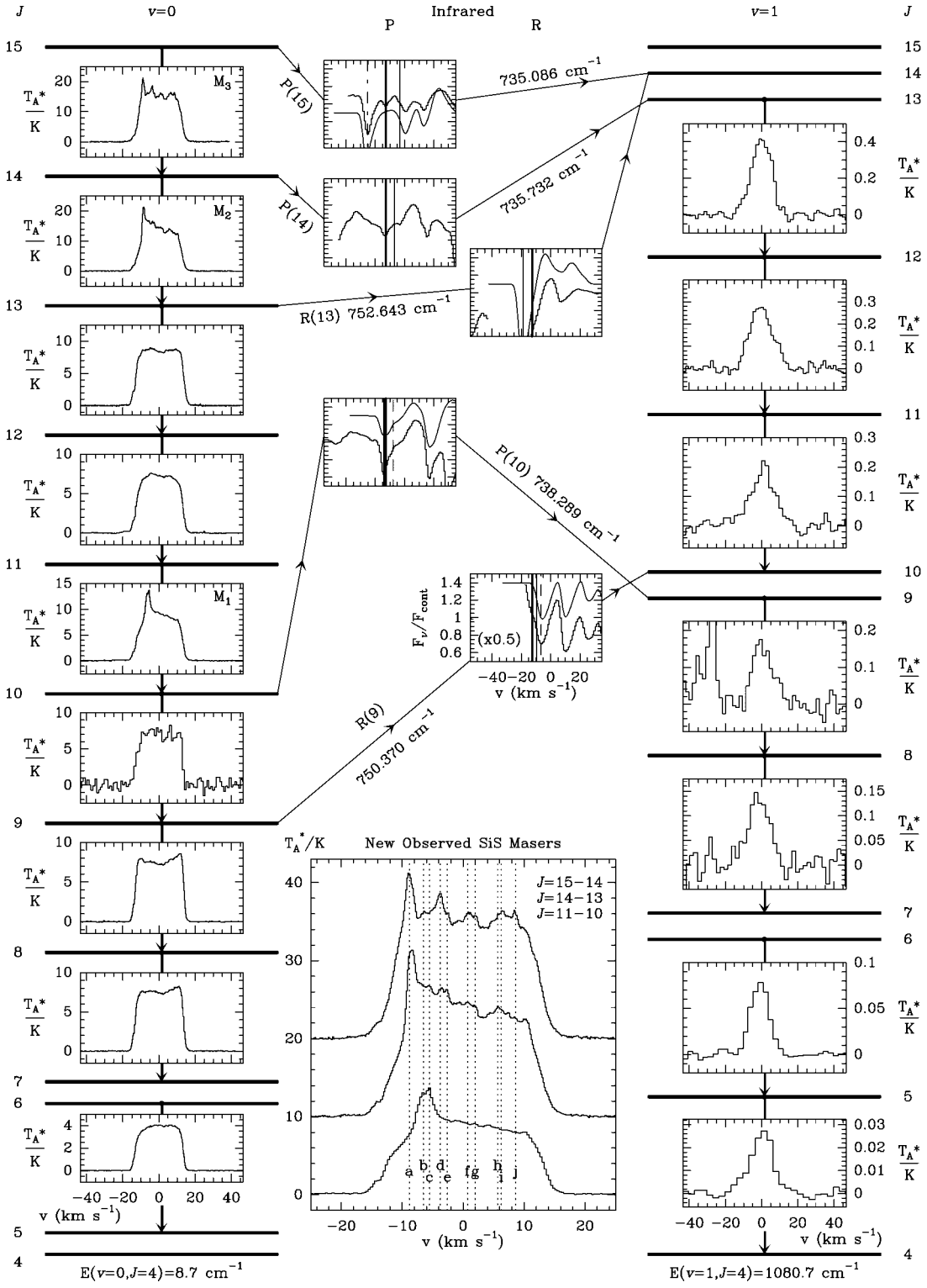

FIG. 1.—Millimeter and mid-IR observations toward IRC +10216. The pure rotational transitions in the $v = 0$ state (*left*) and in the $v = 1$ state (*right*) are plotted as a function of the velocity with respect to the star ($v_{\rm LSR} = -26.5$ km s^{-1}). The velocity structure of the three observed masers M_1, M_2, and M_3 is shown in more detail at bottom center, where the upper lines have been increasingly shifted by 10 K. The middle insets present some mid-IR spectra at the frequencies of several rovibrational $v = 1$–0 SiS lines, whose labels and frequencies are also shown. The zero of the velocity scale is set to the SiS frequency corrected for the local standard of rest. The observed spectrum is plotted as a histogram. The curves above these correspond to a radiative transfer model that only considers C_2H_2, HCN, and their isotopologues (J. P. Fonfría Expósito et al. 2006, in preparation). The vertical lines indicate the position of maximum absorption for the transitions of SiS (*thick lines*), C_2H_2 (*thin lines*), $H^{13}CCH$ (*dot-dashed line*), and HCN (*dashed lines*). [*See the electronic edition of the Journal for a color version of this figure*.]

($R_* = 5 \times 10^{13}$ cm, $T_* = 2300$ K), with $T_k = 1000$ K and $n_{H_2} = 1.6 \times 10^9$ cm^{-3} (mean values for this region derived in J. P. Fonfría Expósito et al. 2006, in preparation) and an expansion velocity of 11 km s^{-1}. We solve the statistical equilibrium for SiS considering 100 rotational levels and three vibrational states and apply the large velocity gradient (LVG) radiative transfer formalism using a code developed by J. Cernicharo. With the assumed n_{H_2}, the column density for H_2 is $\simeq 7 \times 10^{23}$ cm^{-2} and the derived one for SiS is $\simeq 5.0 \times 10^{18}$ cm^{-2}. Hence, the SiS abundance is $\simeq 7 \times 10^{-6}$. The derived abundance is compatible with a high SiS abundance in the innermost CSE (from LTE chemistry models, 3×10^{-5}; Agúndez & Cernicharo 2006), while the SiS abundance farther out in the CSE is considerably lower (6.5×10^{-7} according to observations of $v = 0$ rotational lines over the outer CSE by Bieging & Nguyen-Q-Rieu [1989]).

Most $v = 0$ rotational lines show a rounded or slightly double-peaked profile, with the blue part partially absorbed by cold SiS through the envelope. However, M_1, M_2, and M_3 show a large extra emission in the form of narrow peaks (FWHM = 1–3 km s^{-1}), suggesting that this emission is arising from very small regions. The velocities of these features, within the -10 to 10 km s^{-1} range, indicate that the SiS maser emission arises from different regions located between the star and the inner dust formation zone ($r \simeq 5R_*$), and in the inner acceleration zone itself. The lines M_2 and M_3 have been previously observed by Sahai et al. (1984), but no maser emission was noticed. This could be due either to the limited sensitivity of their observations or to a time variability of the SiS maser phenomenon. The bottom center panel of Figure 1 shows in detail the line profiles of the observed masers. Up to 10 maser features, labeled *a*, …, *j*, are identified. The most complex line profile is that of M_3. It is formed by five main features: *a*, *d*, *f*, *i*, and *j*, with velocities of -8.8, -3.7, 0.88, 6.3, and 8.4 km s^{-1}, respectively. The line profiles show that the strongest peaks are at negative velocities, having their red counterparts rather weak. This behavior was previously found by Henkel et al. (1983) for the $v = 0$ $J = 1$–0 line, which mostly consists of a narrow peak (FWHM = 0.3 km s^{-1}) centered at -13.5 km s^{-1}. The strong asymmetry of the line shapes can be due either to blanking by the star of the redshifted maser or to amplification of the blueshifted emission by the foreground stellar environment.

The strongest observed maser, M_3, with $T_{MB} \simeq 60$ K ($F_{obs} \simeq 300$ Jy, with thermal and nonthermal emission), is weak compared with some SiO masers detected in O-rich stars (e.g., Cernicharo et al. 1993) or HCN masers observed in IRC +10216 (Lucas & Cernicharo 1989; Schilke & Menten 2003). However, M_1, M_2, and M_3 are stronger than the SiS $J = 1$–0 maser observed toward IRC +10216 by Henkel et al. (1983). The similarity between maser features in M_2 and M_3 indicates that they may arise from the same regions and be produced by the same pumping mechanism; the maser in M_1 is probably formed in other regions. Hence, we suggest two possible geometries of the innermost CSE to explain the observed features:

1. There is an onion-like innermost region, where each maser is produced in a shell. This hypothesis is supported by the symmetry of features *a*–*j* and *d*–*i*. The peaks at extreme velocities, *a* and *j*, would be produced just in front of and behind the star (Henkel et al. 1983) near the inner dust formation shell ($r \simeq 5R_*$) with expansion velocities of $\simeq$5–11 km s^{-1}. The features *d* and *i* would be produced in a similar way but in an inner shell with a lower expansion velocity. Finally, the central peak, *f*, would be formed in a shell very close to the star, with the whole shell contributing to the maser emission. M_1 would be produced in a cap-shaped region in front of the star.

2. All the masers are formed at different positions in a clumpy shell. The different features in M_2 and M_3 would be produced in different regions of the shell: peaks *a* and *j* in front of and behind the star, and the other peaks (*d*, *f*, and *i*) in different clumps, as occurs with the only feature of M_1.

The classic pumping mechanism for the SiO $v > 0$ masers observed in O-rich stars resides in the increase of the trapping lifetime $(A/\tau)_{v \rightarrow v-1}$ with J for $v \rightarrow v - 1$ transitions, when they become optically thick (Kwan & Scoville 1974). This mechanism produces masers in adjacent rotational lines of the v state and explains the $v = 1$ and $v = 2$ SiO masers (Bujarrabal & Nguyen-Q-Rieu 1981; Lockett & Elitzur 1992). However, the masers observed in rotational transitions of ^{29}SiO and ^{30}SiO and in $v = 3$ and $v = 4$ of SiO do not show the latter behavior and have been interpreted as due to IR overlaps between rovibrational lines of SiO isotopologues (Cernicharo et al. 1991; González-Alfonso & Cernicharo 1997). For SiS, the absence of maser emission in $v = 1$ rotational lines and the odd $v = 0$ pattern also exclude the Kwan-Scoville pumping mechanism. In addition, Carlström et al. (1990) found an out-of-phase oscillation in the intensity of the SiS lines $v = 0$, $J = 6$–5 and $J = 5$–4. In the latter, the blue- and redshifted peaks at nearly the terminal velocity appear and disappear, indicating that they could be maser features produced by an overlap involving the level $J = 5$. These facts suggest that overlaps of $v = 1$–0 rovibrational transitions of SiS with those of mode ν_5 of C_2H_2 and mode ν_2 of HCN could provide the pumping mechanism. C_2H_2 and HCN are abundant in the inner CSE of IRC +10216 and dominate the 11–14 μm spectrum (J. P. Fonfría Expósito et al. 2006, in preparation). Overlaps with these two species have been already proposed by Sahai et al. (1984) to explain the different profiles of adjacent-J lines of SiS. However, the SiS frequencies used in that work were not as accurate ($\sigma \sim 10^{-1}$ cm^{-1}) as those available today. We have calculated those frequencies from the Dunham coefficients determined by Sanz et al. (2003), for which the error of the band center is less than 10^{-4} cm^{-1} ($\simeq$0.04 km s^{-1}; the relative accuracy of P and R lines is much better). The frequencies of C_2H_2, $H^{13}CCH$, HCN, and $H^{13}CN$ lines have been taken from the HITRAN2004 database (Rothman et al. 2005), with an accuracy better than 10^{-3} cm^{-1} ($\simeq$0.4 km s^{-1}) for C_2H_2 and $H^{13}CCH$, and 10^{-4} cm^{-1} for HCN and $H^{13}CN$.

Table 1 shows the mid-IR line overlaps of SiS with C_2H_2, HCN, and their most abundant isotopologues. For the overlap search, we selected coincidences within $|\Delta v| < 10$ km s^{-1}. However, since the CSE is expanding, every region of the envelope is receding from the others. Hence, if the population of the SiS levels is affected by an overlap with a strong line of another species, the frequency of this overlapping transition must be higher than the SiS one. This would restrict the condition to positive Δv. Nevertheless, because of the line width, lines at $\Delta v < 0$ can overlap the SiS lines. Hence, we have set the negative cutoff to one-half the typical line width in the innermost CSE ($\simeq$5 km s^{-1}; J. P. Fonfría Expósito et al. 2006, in preparation). Therefore, our search is restricted to -2.5 km s$^{-1} \leq \Delta v \leq 10$ km s^{-1}. All the rovibrational SiS lines commented on hereafter refer to $v = 1 \rightarrow 0$ transitions and will be labeled with the usual spectroscopic nomenclature *R*, *Q*, *P* (see note to Table 1).

TABLE 1

MID-INFRARED LINE OVERLAPS OF SiS WITH C_2H_2, HCN, AND THEIR MOST ABUNDANT ISOTOPOLOGUES

Line	ν (cm^{-1})	Molecule	Transition	Δv (km s^{-1})
Overlaps Involving SiS Levels of Observed Lines				
$R(9)$	750.3695	HCN	01^10–00^00 $R_e(12)$	−6.6
$P(10)$	738.2889	C_2H_2	$1^{-1}1^1$–$1^{-1}0^0$ $R_f(3)$	1.2
$R(13)$	752.6431	C_2H_2	0^01^1–0^00^0 $R_e(9)$	5.9
$P(14)$	735.7324	C_2H_2	0^01^{-1}–0^00^0 $Q_e(38)$	−6.1
$P(15)$	735.0861	C_2H_2	0^01^{-1}–0^00^0 $Q_e(36)$	−9.9
Overlaps Involving SiS Levels of Unobserved Lines				
$P(2)$	743.2624	C_2H_2	0^01^1–0^00^0 $R_e(5)$	0.6
$P(16)$	734.4368	C_2H_2	0^01^{-1}–0^00^0 $Q_e(34)$	1.1
$P(20)$	731.8114	C_2H_2	0^01^{-1}–0^00^0 $Q_e(24)$	9.5
$P(22)$	730.4815	C_2H_2	$1^{-1}1^1$–1^10^0 $Q_e(18)$	−2.1
$R(22)$	757.5819	C_2H_2	1^11^1–1^10^0 $R_e(10)$	0.1
		$H^{13}CN$	01^10–00^00 $R_e(17)$	5.2
$P(23)$	729.8123	$H^{13}CCH$	0^01^{-1}–0^00^0 $Q_e(19)$	8.7
$P(24)$	729.1402	C_2H_2	0^01^{-1}–0^00^0 $Q_e(1)$	9.4
$P(25)$	728.4654	$H^{13}CCH$	0^01^{-1}–0^00^0 $Q_e(7)$	−0.0
$R(25)$	759.1733	HCN	01^10–00^00 $R_e(15)$	3.6
$R(26)$	759.6977	C_2H_2	0^01^1–0^00^0 $R_e(12)$	−1.0
$R(33)$	763.2816	$H^{13}CN$	01^10–00^00 $R_e(19)$	6.1
$P(38)$	719.4363	C_2H_2	1^11^1–1^10^0 $P_e(5)$	4.5
$R(40)$	766.7130	C_2H_2	0^01^1–0^00^0 $R_e(15)$	4.3
$R(42)$	767.6652	C_2H_2	1^11^{-1}–1^10^0 $R_e(20)$	8.7
$R(45)$	769.0697	C_2H_2	0^01^1–0^00^0 $R_e(16)$	−1.8
$P(48)$	712.1720	C_2H_2	$1^{-1}1^{-1}$–$1^{-1}0^0$ $P_f(8)$	4.7

NOTE.—Overlaps of SiS with C_2H_2, $H^{13}CCH$, HCN, and $H^{13}CN$ found in the mid-IR range 690–780 cm^{-1} with -2.5 km $s^{-1} \leq \Delta v \leq 10$ km s^{-1}, where $\Delta v/c = [\nu(X) - \nu(\mathrm{SiS})]/\nu(\mathrm{SiS})$ and $J \leq 50$ (corresponding to SiS $v = 0$ rotational frequencies below 900 GHz). The lines and frequencies at the left correspond to the vibrational transitions $v = 1 \rightarrow 0$ of SiS. The errors on the velocities are less than 0.5 km s^{-1}. The notation for the C_2H_2 and $H^{13}CCH$ vibrational states involved in the rovibrational transitions is $v_4^{l_4}v_5^{l_5}$, whereas for HCN and $H^{13}CN$ it is $v_1v_2^{l}v_3$. The parity of the lower level is even (e) or odd (f). The transitions are labeled as R, P, and Q for $J_{up} - J_{low} = +1, -1, 0$.

In order to qualitatively interpret the effects of IR overlaps on maser emission, we have used the same LVG radiative transfer code, modified to account for overlaps, changing the intensity at the overlapping frequency and the escape probability for photons from the overlapped lines. Thus, for some SiS lines the excitation temperature becomes negative (maser activation) and the brightness temperature is considerably enhanced. M_2 and M_3 are naturally explained by the overlap of the $R(13)$ line of SiS with the strong C_2H_2 line 0^01^1–0^00^0 $R_e(9)$ (Table 1). SiS molecules are easily excited from $v = 0$, $J = 13$ to $v = 1$, $J = 14$ through $R(13)$ and decay to $v = 0$, $J = 15$ via $P(15)$, creating a population inversion between $v = 0$ $J = 13$ and $J = 15$ and producing maser emission in M_2 and M_3. M_1 may be produced by the overlap of the $P(10)$ SiS line with the strong C_2H_2 line $1^{-1}1^1$–$1^{-1}0^0$ $R_f(3)$. This overlap can pump SiS molecules from $v = 0$, $J = 10$ to $v = 1$, $J = 9$ through $P(10)$, thus depopulating the $v = 0$, $J = 10$ level and producing the inversion between $v = 0$ $J = 10$ and $J = 11$.

We have also looked for overlaps of $v = 1$–0 higher J SiS lines with C_2H_2 and HCN transitions to try to predict SiS masers at submillimeter wavelengths. Some of them are shown in the bottom of Table 1. They suggest, for example, that a maser could be found in rotational transitions involving the $v = 0$, $J = 23$ level (likely $J = 24$–23 and maybe 23–22), or the $v = 0$ $J = 25$ and $J = 26$ states (perhaps in the $v = 0$, $J = 27$–26 and maybe 26–25). These overlaps could also produce masers in $v = 1$ rotational transitions.

There are many overlaps of other SiS isotopologues with lines of C_2H_2, HCN, and $^{28}Si^{32}S$. With the adopted criteria for the overlap search (see note to Table 1), we have found 91, 93, 76, and 94 coincidences for ^{29}SiS, ^{30}SiS, $Si^{34}S$, and $Si^{33}S$, respectively. Consequently, although these species are less abundant than $^{28}Si^{32}S$, the population of some levels could be inverted, producing maser emission.

This study represents the discovery of three new SiS masers and should be complemented with future observations of higher J, $v = 0$ and $v = 1$ rotational transitions. Furthermore, a detailed multimolecule nonlocal radiative transfer model would help to understand the dust formation region and the role of SiS in C-rich evolved stars.

We would like to thank M. J. Richter (NSF grant AST 03-07497), J. H. Lacy (NSF grant AST 02-05518), and collaborators for providing us with the mid-IR observations.[1] We also thank our referee for valuable comments, and the Spanish Ministerio de Educación y Ciencia for funding support through grants ESP 2004-665 and AYA 2003-2785, and the "Comunidad de Madrid" government under PRICIT project S-0505/ESP-0237 (ASTROCAM). This study is supported in part by the European Community's Human Potential Program under contract MCRTN-CT-2004-51230, "Molecular Universe."

[1] Visiting Astronomer at the Infrared Telescope Facility, which is operated by the University of Hawaii under cooperative agreement NCC 5-538 with the National Aeronautics and Space Administration, Science Mission Directorate, Planetary Astronomy Program.

REFERENCES

Agúndez, M., & Cernicharo, J. 2006, ApJ, in press (astro-ph/0605645)
Bieging, J. H., & Nguyen-Q-Rieu. 1989, ApJ, 343, L25
Bujarrabal, V., & Nguyen-Q-Rieu. 1981, A&A, 102, 65
Carlström, U., Olofsson, H., Johansson, L. E. B., Nguyen-Q-Rieu, & Sahai, R. 1990, in From Miras to Planetary Nebulae, ed. M. O. Mennessier & A. Omont (Gif-sur-Yvette: Ed. Frontières), 170
Cernicharo, J. 1985, ATM: A Program to Compute Atmospheric Opacity between 0 and 1000 GHz (IRAM Rep. 52) (Grenoble: Inst. Radioastron. Millimétrique)
Cernicharo, J., Bujarrabal, V., & Lucas, R. 1991, A&A, 249, L27
Cernicharo, J., Bujarrabal, V., & Santarén, J. L. 1993, ApJ, 407, L33
Cernicharo, J., Guélin, M., & Kahane, C. 2000, A&AS, 142, 181
Elitzur, M. 1992, ARA&A, 30, 75
González-Alfonso, E., & Cernicharo, J. 1997, A&A, 322, 938
Gray, M. 1999, Philos. Trans. R. Soc. London A, 357, 3277
Henkel, C., Matthews, H. E., & Morris, M. 1983, ApJ, 267, 184
Keady, J. J., & Ridgway, S. T. 1993, ApJ, 406, 199
Kwan, J., & Scoville, N. 1974, ApJ, 194, L97
Lacy, J. H., Richter, M. J., Greathouse, T. K., Jaffe, D. T., & Zhu, Q. 2002, PASP, 114, 153
Lockett, P., & Elitzur, M. 1992, ApJ, 399, 704
Lucas, R., & Cernicharo, J. 1989, A&A, 218, L20
Monnier, J. D., Geballe, T. R., & Danchi, W. C. 1998, ApJ, 502, 833
Pardo, J. R., Alcolea, J., Bujarrabal, V., Colomer, F., del Romero, A., & de Vicente, P. 2004, A&A, 424, 145
Pardo, J. R., Cernicharo, J., González-Alfonso, E., & Bujarrabal, V. 1998, A&A, 329, 219
Pardo, J. R., Cernicharo, J., & Serabyn, G. 2001, IEEE Trans. Antennas Propag., 49, 1683
Rothman, L. S., et al. 2005, J. Quant. Spetrosc. Radiat. Transfer, 96, 139
Sahai, R., Wootten, A., & Clegg, R. E. S. 1984, ApJ, 284, 144
Sanz, M. E., McCarthy, M. C., & Thaddeus, P. 2003, J. Chem. Phys., 119, 11715
Schilke, P., & Menten, K. M. 2003, ApJ, 583, 446
Schöier, F. L., Olofsson, H., & Lundgren, A. A. 2006, A&A, 454, 247